Detection of Partially Coherent Optical Emission Sources

Ricardo C. Coutinho[a,b], David R. Selviah[a] and Herbert A. French[a]

[a]University College London, Department of Electronic and Electrical Engineering, Torrington Place, London WC1E 7JE, United Kingdom

e-mail:r.coutinho@ee.ucl.ac.uk; d.selviah@ee.ucl.ac.uk

Tel: +44 20 7679 3056

[b]Brazilian Navy

ABSTRACT

Detection of airborne optical emission sources in Infrared Search and Track (IRST) systems is usually carried out using the blackbody temperature or emissivity difference between the emission source and the background. Recent countermeasure techniques include emissivity tailoring and temperature distribution tailoring across the emission source area to avoid the formation of "hot spots" which effectively embeds the emission source in its background. A technique relying on coherence rather than irradiance is presented, allowing detection with poor signal-to-clutter ratios.

The technique has some similarity with Fourier Transform Spectroscopy (FTS), and its key components are a Michelson interferometer, which measures the coherence profile of the scene in the field of view, and an interference filter, which uses the background illumination to create amplitude minima in the interferogram envelope. Unlike FTS, the interferometer moving mirror scans only a tiny portion of the interferogram, this being the region surrounding the first minimum of its envelope. It is shown that this envelope is a sinc function, and that at this minimum the phase of the interferogram undergoes a π phase step, which is used to define the position accurately. When a partially coherent emission source comes into the field of view, the modulus of the net complex degree of coherence of the scene increases, and the phase step position changes; this latter optical feature is used to declare detection.

We present a simple theoretical model and compare it with experimental results for highly emissive sources having various coherence lengths in the presence of incoherent background illumination. Agreement between the experimental results and the theory is discussed.

KEYWORDS: spectral signature; clutter rejection; pattern recognition; temporal coherence; optical interferometry.

1. INTRODUCTION

It is commonly required to detect a hot or coloured object in surroundings of a different temperature or colour. The spectral signature of the object in emitted, transmitted or reflected light must be distinguished from the somewhat higher energy, having a different spectrum, coming from the background and surroundings. This is a pattern recognition problem where the signal is buried in noise. If the object is emitting more energy than its local surroundings then this can be detected using spatial power

measurements. However, in some cases the object may emit the same or less energy than its local surroundings or its emissions may be suppressed, for example, by the use of special coatings to reduce the emissivity[1], and by cooling the hot exhaust gases from engines or turbines[2]. These suppression measures aim to embed the emission source in the background, increasing the sensitivity requirements of the detection system.

The techniques based on detecting local spatial power concentrations do not take advantage of all of the information[3] carried in the optical beam such as temporal, spectral, coherence and polarisation data. A spatial spectral mapping identifies sources with different colour characteristics than the local surroundings. However, the formation of spectral maps in real time may give too much data from which the required information must be extracted. If the problem is only to identify quickly whether a source exists within the field of view of the detection instrument then a simpler, more direct approach can be used.

This paper describes a detection technique based on the coherence properties of the optical signal rather than on its intensity. It does not make use of the spectral properties directly but takes account of them indirectly in the coherence interferogram. Section 2 briefly outlines the principle of the approach[4, 5]; section 3 contains a simple mathematical model. In section 4 laboratory experiments conducted in the visible band are described, together with the signal processing algorithm developed to aid recognition of features. The results of the experiments are presented and their agreement with the theory is discussed in section 5, whilst section 6 concludes summarising the achievements.

2. PRINCIPLE

Our approach is similar to Fourier Transform Spectroscopy (FTS) in that the incoming signal is fed to an interferometer having a mirror in one path, which scans along the optic axis. However, unlike FTS, our path difference scan is much shorter and hence, faster. In addition, in our technique no Fourier transform is required, as the changes in the signal spectrum are sensed by examining the interferogram rather than the spectrum. The main components are (figure 1):

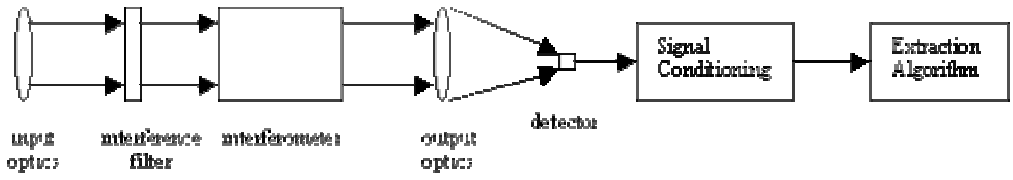

Figure 1 - Generic System Block Diagram

- an interference filter is used to limit the background spectrum to the region of interest, and more importantly to generate an optical *feature*. The feature is recognised and located in time and any change in its temporal position is used to declare detection. The self-coherence function of the incoming radiation is the Fourier transform of the power spectrum[6]. So an input filter with a very steep spectral roll-off characteristic, resembling a top-hat function, will produce a sinc-like coherence profile or interferogram. This is the envelope of an enclosed carrier (the interference fringes). The first null of this function is chosen to be the *feature* of interest. The position of the first null along the path difference axis is recorded as a reference value when no emission source is present. In this situation, assuming that the background power spectral density is constant across the filter bandwidth, it can be shown[5] that this position equals the reciprocal of the filter bandwidth. If an emission source is present, however, and if it contains a narrow spectral feature

encompassed within the filter bandwidth, the net degree of coherence changes, and the null feature moves, as will be shown in the next section;

- an interferometer, which performs the auto-correlation operation required to compute the net degree of coherence of the radiation in the Instantaneous Field of View (IFOV); and

- an algorithm capable of recognising and tracking the position of the optical feature used as the event marker. The zero-crossing in amplitude of the sinc function causes a 180° phase reversal in the carrier. To achieve higher discrimination, rather than detecting the null by recognising the minimum amplitude the algorithm recognises this phase step and registers its position along the path difference axis. The magnitude of any measured phase step shift must then be compared with a threshold as in a conventional decision process. Further details of the algorithm are presented in section 4.

3. THEORETICAL MODEL

In this section we describe a simple model which has idealised emission source spectral characteristics and idealised input filter characteristics but is nevertheless useful to assess the sensitivity of the system. We assume that the background power spectral density is constant across the interference filter bandwidth. Also, the frequency response of this filter is assumed to be a top hat function of unity amplitude, bandwidth $\Delta\kappa$ and centred at κ_0, both expressed in wavenumbers (the reciprocal of wavelength). P_B is the background total power after filtering. The emission source is assumed to have a Gaussian spectral profile, with a total power P_E and Full Width Half Maximum (FWHM) δ. Thus, considering only the direct radiation from the emission source and the background, the net power spectrum after the interference filter will be:

$$S(\kappa) = B(\kappa) + E(\kappa) = rect\left(\left|\kappa - \kappa_0\right| / \Delta\kappa\right)\left\{P_B / \Delta\kappa + \left(P_E \cdot \alpha / \sqrt{\pi}\right) e^{-\alpha^2(\kappa-\kappa_0)^2}\right\} \quad (1)$$

where α is a factor inversely proportional to δ, $B(\kappa)$ is the filtered background power spectrum, and $E(\kappa)$ is the filtered emission source power spectrum. $S(\kappa)$ is shown in figure 1.

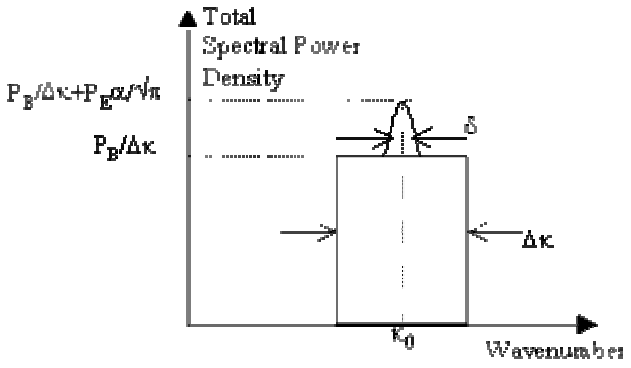

Figure 2 - Emission Source and Background Power Spectrum

Fourier transforming (1) and integrating the power spectral density across the filter bandwidth gives the Self-Coherence Function of the radiation that reaches the detector:

$$\Gamma(\tau) = P_B\left\{sinc(\pi\tau\Delta\kappa) + PR.erf\left(1.176.\Delta\kappa/\delta\right)e^{\frac{\pi^2}{4\ln 2}\delta^2\tau^2}\right\}e^{-j2\pi\kappa_0} \quad (2)$$

where $PR=P_E/P_B$ is the ratio of the emission source total power and the background total power after passing through the interference filter, *erf* is the error function, representing the effect of the filter on the emission source spectrum, and α has been expressed as a function of δ . This equation shows a carrier modulated by an envelope, which is a combination of the influences of the filter and the emission source spectra. A 180° phase step in the carrier occurs when the envelope function has a zero crossing. Hence, in order to recognise and locate this feature, only the envelope function needs to be analysed. The term in {} brackets of equation (2) was evaluated using a computer program, and the phase step position was found numerically for various power ratios. The resulting curves are presented together with the experimental results in section 5.

4. EXPERIMENTAL SYSTEM

The visible band was chosen for the initial experiments for convenience and ease of alignment. The experimental system to measure the shift in the phase step position is shown in figure 3. Two light sources simulate the emitter and the background. The light from these sources is collimated using 30mm f/2 plano-convex lenses to simulate emissions from distant objects and the environment. Neutral density filters are used to adjust the power ratio. The two sources are combined through a 50:50 cube beamsplitter. The combined output enters 'the detection system' where it passes through a narrow band interference filter. The central wavelength of the filter?s passband changes with the angle of incidence so the filter is mounted on a rotation stage, which is adjusted to align the emission and filter central wavelengths. The filtered radiation is sent to a Michelson interferometer. In the interferometer the light is split at another beamsplitter. The transmitted radiation reflects from a fixed mirror while the remaining radiation reflects from a scanning mirror, which is moved in increments along the optical path to vary the phase delay. The two reflected beams recombine in the same beamsplitter. The interferometer acts as an auto-correlator, where the correlation delay is given by twice the path difference between the beams. The moving mirror is translated by a stage driven by a stepper motor with a resolution of 0.1 μ m, which is powered by a Klinger MD4 driver controlled by a Klinger MC4 controller. The controller is connected to a computer through an IEEE 488 interface, from whence it receives its commands and sends back position information. The computer program is set to scan the mirror position in a linear manner from one extreme to the other before it returns to its starting position and repeats the motion in a succession of ramps. The length of the scan, the scan speed and the number of scans are programmable. The majority of the measurements were taken using a 10 μ m scan, corresponding to 20μ m path difference range, with a speed of 50 μ m/sec in steps of 0.1μm.

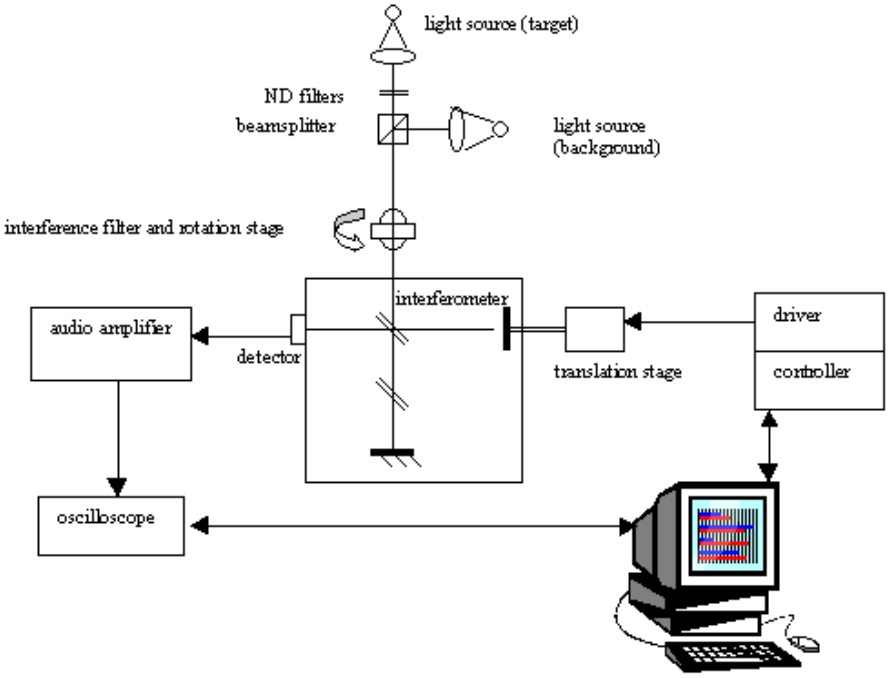

Figure 3 - Laboratory Set-up

A silicon photodetector is placed at the output of the interferometer. The output radiation is already collimated so the detector active area ($1cm^2$) scans the fringes which alternate dark and light as the mirror scans. The electrical signal so generated is filtered and amplified by 30 dB in an audio amplifier. The speed of the scan allows the determination of the mean frequency in the range 150 to 160 Hz for the wavelength range used in the experiments (630 to 680 nm). The mirror scanned at around 2Hz. So the analogue filter?s 3 dB cut-off frequencies were set to 100 Hz and 10 kHz. A digital oscilloscope acquires this signal with AC coupling at a sampling frequency of 5.12 kHz. This also substantially removed the DC level. The translation stage suffered from hystheresis so only one of the directions of the scan was used. Each 20 μ m path difference range gave a data block of 1024 samples, which was then transferred to the computer using the IEEE 488 interface for off-line processing.

A typical 1024 sample data block is depicted in figure 4. An off-line signal-processing algorithm is required to determine the position of the signal?s phase transition. The algorithm was implemented using Matlab to ease its development at this stage. Two data blocks are loaded and processed in parallel, one recorded without any emission source, and another with the emission source. The data is time gated to exclude the noise recorded while the translation stage is reversing. This region is shown to the left of the plot in figure 4. Any remaining DC level is removed by subtracting the global average from the data. The average carrier frequency is found by counting the number of zero crossings of the signal per second. This carrier frequency is used to calculate the 3dB points of a software Butterworth bandpass filter signal processing routine, which filters the data. The 3dB points are set unequally to 0.8 and 2.2 times the carrier frequency. This permits the recovery of the phase step, which has high frequency content depending on the rise time of the step. The filtered signal is phase and frequency demodulated using the

same carrier frequency by means of two software demodulation routines. The position of the phase step is found in the frequency-demodulated plot by selecting the frequency spike with maximum amplitude. The difference in sample numbers between the two positions (with and without emission source) is multiplied by a factor to convert it to microns and is then displayed as the phase step shift. The program also generates plots of the two signals as they go through the processing steps, and one example is shown in figure 5. For each plot, the lower curves correspond to no emission being present while the upper ones have an emission and background radiation. The shift in the feature?s position can be seen in the frequency plot.

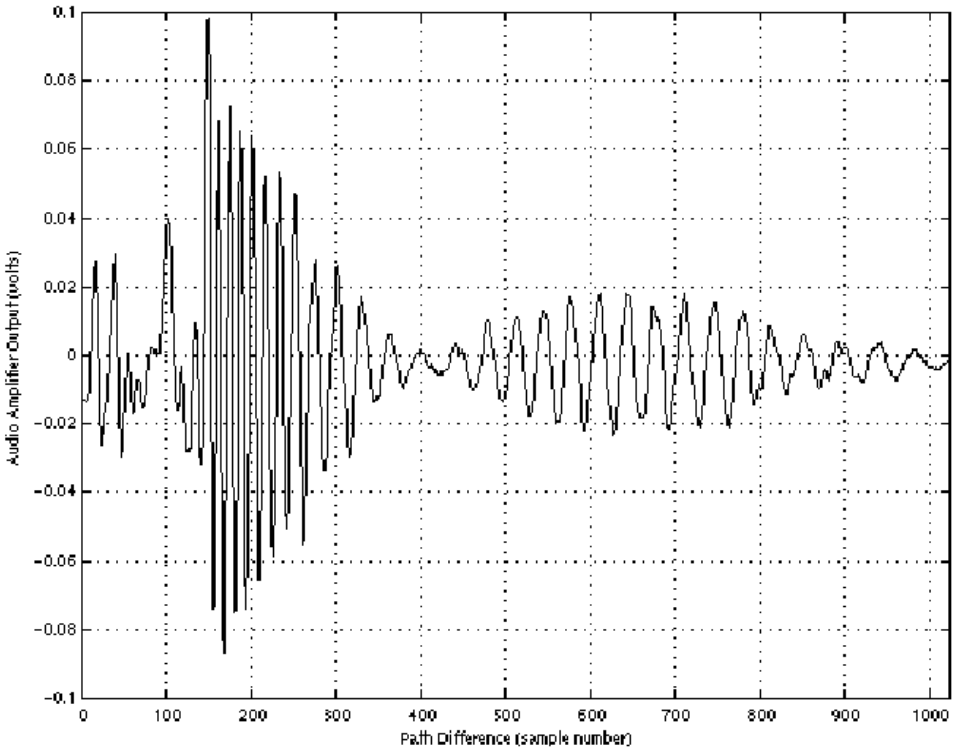

Figure 4 - A Data Block Showing the Phase Step Region

5. EXPERIMENTAL METHOD AND RESULTS

Three combinations of emission source and filter were used to assess the change in sensitivity due to different emission source to filter bandwidth ratios. One employed an essentially coherent emission source (gas laser), and the other two used partially coherent emission sources of different coherence lengths. In all of the measurements a 20W-quartz halogen lamp with a blackbody temperature of 3200K was used as an effectively white light background. Such a lamp suffers from 100Hz modulation arising from the electrical supply but our filtering served to reduce this to give an acceptable phase step shift error of less than 0.2microns. In one of the experiments a second, similar lamp was first filtered and was then used as the emission source. These combinations are presented in table 1, and the total powers of the various sources

after filtering are shown in table 2.

Emission Source	Central Wavelength (nm)	FWHM (nm)	Filter	Central Wavelength (nm)	FWHM (nm)	Bandwidth Ratio After Filtering
5 mW He-Ne Laser	632.8	0.002	Interference Filter	632.6	11	$1.818.10^{-4}$
20W quartz halogen lamp through interference filter	648.7	12.2	Interference Filter (tilted to match central wavelength)	651.9	36.2	0.337
InGaAlP 15000 mcd LED	644	18	Interference Filter (tilted to match central wavelength)	651.9	36.2	0.497

Table 1 - Optical Sources and Interference Filters used in the experiments

Source	Power Range
5 mW He-Ne Laser	0.935 nW - 2.77 μ W
20W quartz halogen lamp through interference filter	39.9 nW - 10.5 μ W
InGaAlP 15000 mcd LED	1.91μ W - 50.84 μ W
20W quartz halogen lamp (background)	32.5 μ W - 145.5 μ W

Table 2 - Power Range of the Optical Sources used in the experiments

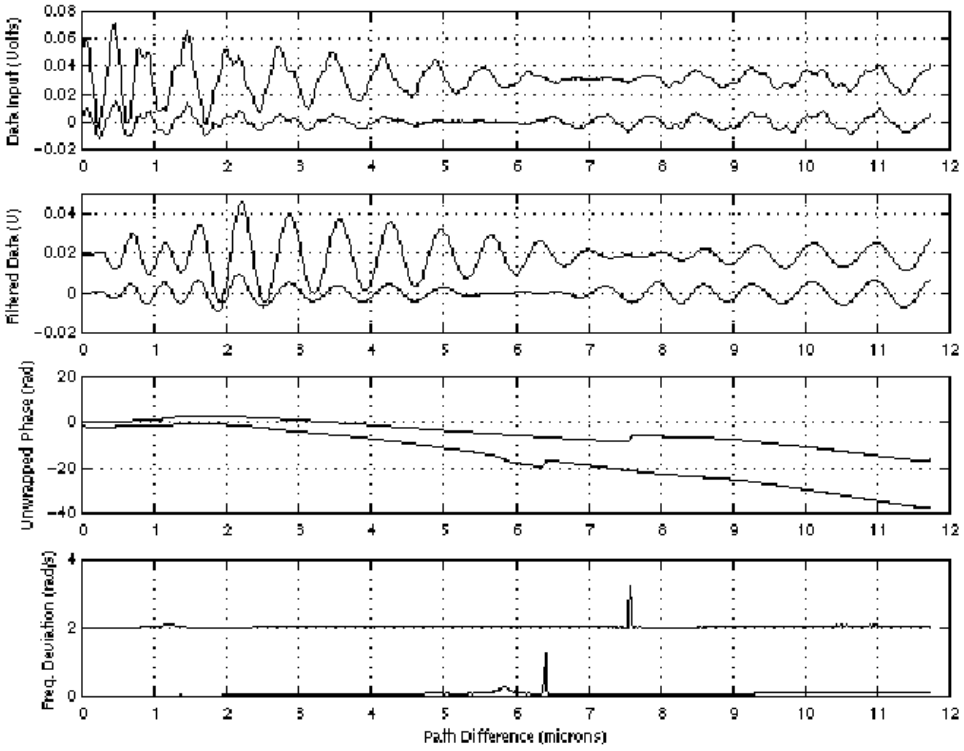

Figure 5 - Off-line Post Detector Processing

The system in figure 3 was aligned to give interference fringes from both sources in the detector plane. Neutral density filters were used either in the emission source or background paths in order to bring the output powers to a ratio where the phenomena to be studied could be observed. Too low a ratio of emission source to background radiation would not produce any measurable shift. Too high a ratio would make the phase step no longer observable, as the sinc function from the filter in the coherence domain is raised by the emission source's Gaussian profile (equation 2), and no longer touches zero. This represents a 'cut-off' of the observability. The LED also allowed the possibility to vary the supply current in order to obtain variable power. Ten different power ratios were recorded using the laser as the emission source. The translation stage suffered from backlash and, in addition, the intensity of both the laser and background lamp varied slowly over time. So, in order to calculate each point, five pairs of readings were taken. One reading of each pair was taken with the emission source and the background and one with only the background. This allowed the difference to be established to remove any slow fluctuations. The mean and standard deviation could then be found from the five calculated phase step shifts. Also, depending on the signal-to-noise ratio, up to 30 data blocks over 30 scans were averaged at the oscilloscope before transferring to the computer. Seven different power ratios were recorded for both of the LED and filtered white light emission sources.

The results for the each combination are shown together with the curves plotted using the simple theory of equation 2, are shown in figures 6, 7 and 8 for the laser, filtered white light and LED respectively. The power ratios along the horizontal axis were measured after filtering in order to allow a comparison with the theory. Thus, we can define two power ratios: one is this ratio after filtering, and the other is the system input power ratio, measured before filtering, and useful for system comparison purposes. The filter generally has the effect to cut out more background power than emission source power so the input power

ratio is somewhat lower than the filtered power ratio plotted would indicate, giving improved detection sensitivity compared to that measured.

The large error bars were due to the lack of repeatability of the translation stage, system noise, the spectral fluctuations of the sources, and false phase steps detected by the algorithm. When the laser is used (figure 6), a high sensitivity was achieved5. Eight of the ten points agree with the simple theory to within one standard deviation. The agreement is poorer at the higher power ratios. Interestingly, if a fitting factor is applied to the term corresponding to the emission source in equation 2, the agreement becomes very good. Clearly further refinement of our model is required to account for this. The maximum phase step shift before cut-off in the experiment was 13.76 microns and so the curve stops here. Higher power ratios than -10.69 dB result in no intersection of the self-coherence function and the axis. The minimum detectable filtered power ratio was -30.38 dB, after which all of the error bars are above zero. This corresponds to an input power ratio of -49.49 dB. The input dynamic range after the filter is then 30.38-10.69=19.69 dB.

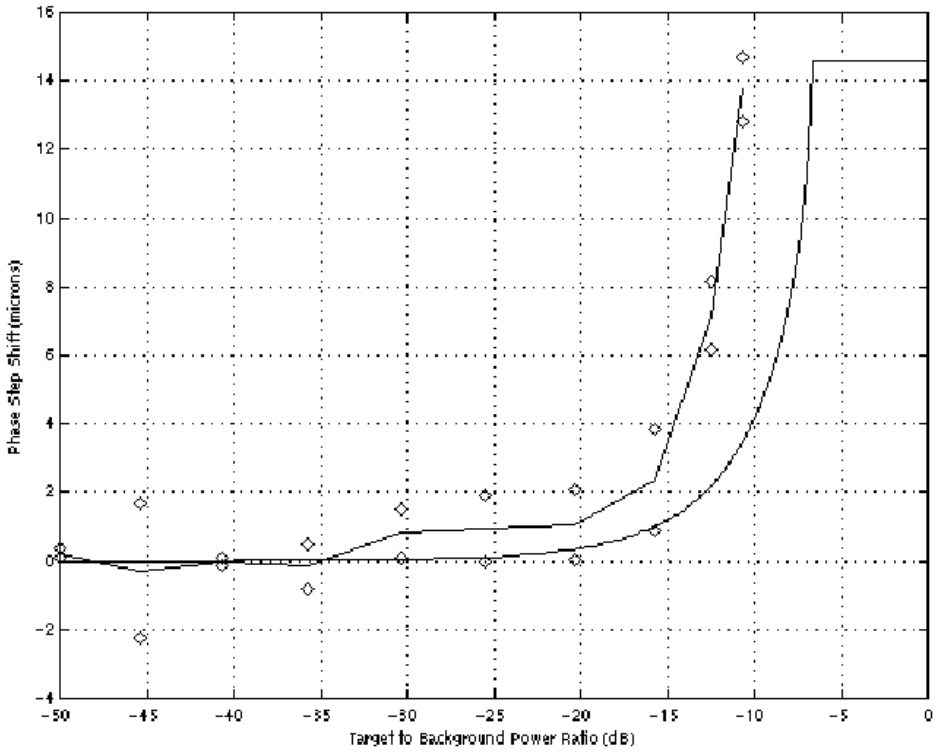

Figure 6 - Laser Emission Source response (bandwidth ratio=0.1818.10^{-4})

When using the filtered white light emission source (figure 7), six of the seven points agree with the theory. The error bars at both high and low power ratios are large, due to noise, as the filtered white light source also suffers from temporal fast and slow fluctuations in addition to those in the background. At the power ratio of -9.67dB there is the additional 'cut-off" problem of the filter's sinc function just touching zero,

which results in large variations in the position of the phase for small lamp intensity fluctuations. Again, the same fitting factor brings the curves into a very good agreement. The minimum detectable filtered power ratio, using the same criteria, with the error bars all above zero, was -20.39 dB, corresponding to an input power ratio of -31.96 dB. The maximum shift was 2.89 microns, although according to the theory it could have gone up to 4.5 microns. The input dynamic range is 20.39-9.67=10.72 dB.

With the LED emission source (figure 8) only one point agreed with the theory; the maximum shift was 1.06 microns, and the minimum detectable filtered power ratio was -5.85 dB, corresponding to an input power ratio of -24.62 dB. The input dynamic range was 4.28 dB. A different fitting factor, less than unity, is required to bring agreement between theory and experiment, in this case.

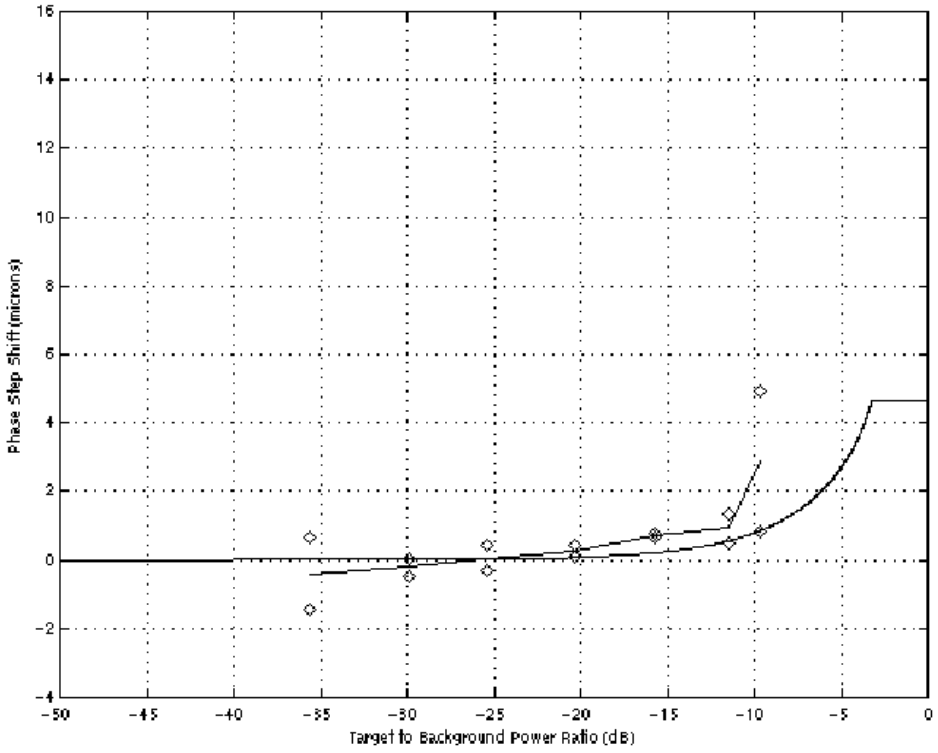

Figure 7 - Filtered white light emission source response (bandwidth ratio=0.337)

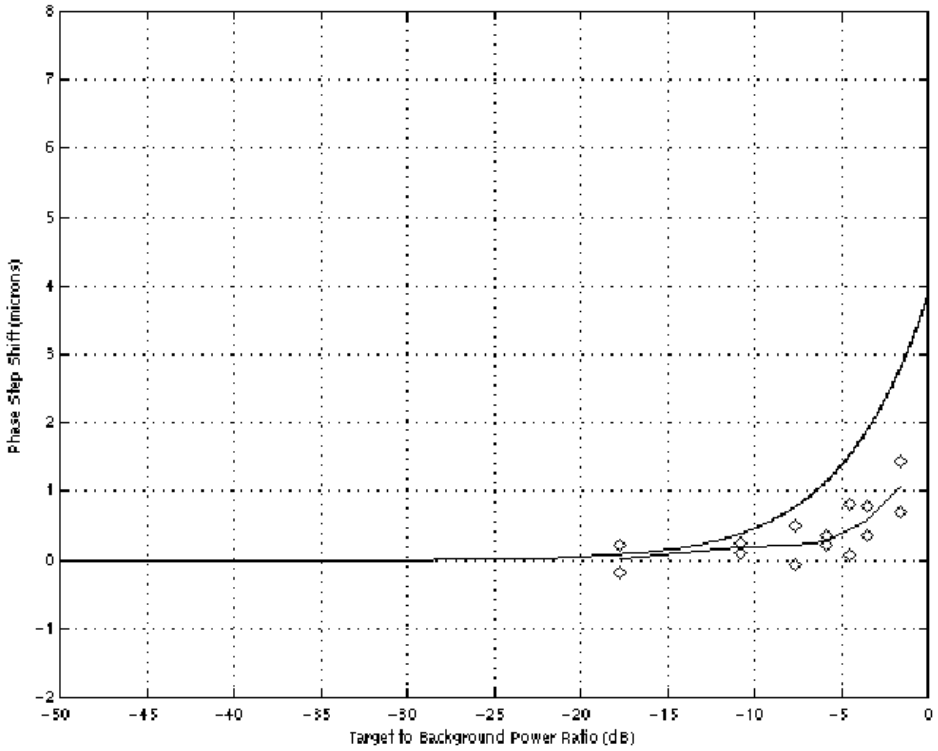

Figure 8 - LED emission source response (bandwidth ratio=0.497)

Figure 9 displays the three sets of experimental measurements on the same graph. The sensitivity monotonically decreases with increasing bandwidth ratio. The power ratios where the curves overlap are in the range of -17.77 to -9.67 dB. Within this range for two power ratios the values of the three curves were noted and replotted in figure 10. There is a much larger increase in the phase step shift with power ratio for the laser. Although we plotted the curves against the emission source to filter bandwidth ratio in an attempt to equalise the effect of different filter bandwidths, it is important to notice that the laser is 4 orders of magnitude narrower than the bandwidth of the other two sources. Therefore, the same change in power ratio will result in a much larger increase in the laser emission source?s intensity.

We now discuss the possible causes of error. In the case of the LED as the model used the typical spectral data supplied by the manufacturer, specific variations from this spectrum were possibly the cause of the poor agreement between theory and experiment. The specification states that the linewidth is 18 nm FWHM at a current of 20 mA, and a temperature of 25°C. During the measurements the current varied between 5 and 30 mA, and the temperature was not controlled. Some other factors possibly affected all the measurements:

- The filter's spectra are not rectangular and have a finite roll off towards the edge of the band. In order to achieve a very high finesse, the variations in the reflectivity of the Fabry-Perot cavity mirrors cause dips and peaks in the passband, thus altering the degree of coherence of the filtered background, and the position of the phase step taken as a reference;

- All of the spectral characteristics presented in table 1 were taken as given by the manufacturers, measured under certain conditions;

- The method used to make the central wavelength of the emission source and background coincide does not guarantee this coincidence, but only that the integrated power from the emission source through the interference filter is maximum;

- The model assumes that the attenuation of the interferometer is the same for the laser, at a specific wavelength, and for all other sources, integrated in the filter bandwidths. As the silicon photodetector has a non-flat frequency response, this alters the measured power ratio;

- The white light spectral radiance has a slope of +3.6% within the passband of the 11nm wide filter, and of +8.7% within the passband of the 36.2 nm wide filter, as calculated using the Planck equation for a blackbody temperature of 3200K, and this was not taken into account in the theory;

- The translation stage used to scan the interferometer?s mirror has a non-zero repeatability. Even with the experimental method used, always measuring the phase step shift in pairs of waveforms, one with and one without the emission source, the problem still occurred. The measurements taken of the position of the phase step without a emission source, within 5 minutes, had a standard deviation of 0.2μm;

- The recognition procedure involves two steps: (i) Choose the largest frequency spike, (ii) Measure the shift of this spike and if it is more than some threshold then the presence of an emission source is detected. The computer algorithm missed the phase step in some waveforms, and pointed to a frequency spike caused by noise, and not by the signal phase step, in others. Of the 256 waveforms recorded, 9 presented no frequency spike, and 11 had larger frequency spikes arising from noise. Considering the measurement of the shift of the correct frequency spike, and not the detection of the emission source itself, we can define a probability of location of 96.48%, and a probability of wrong location of 4.3 %.

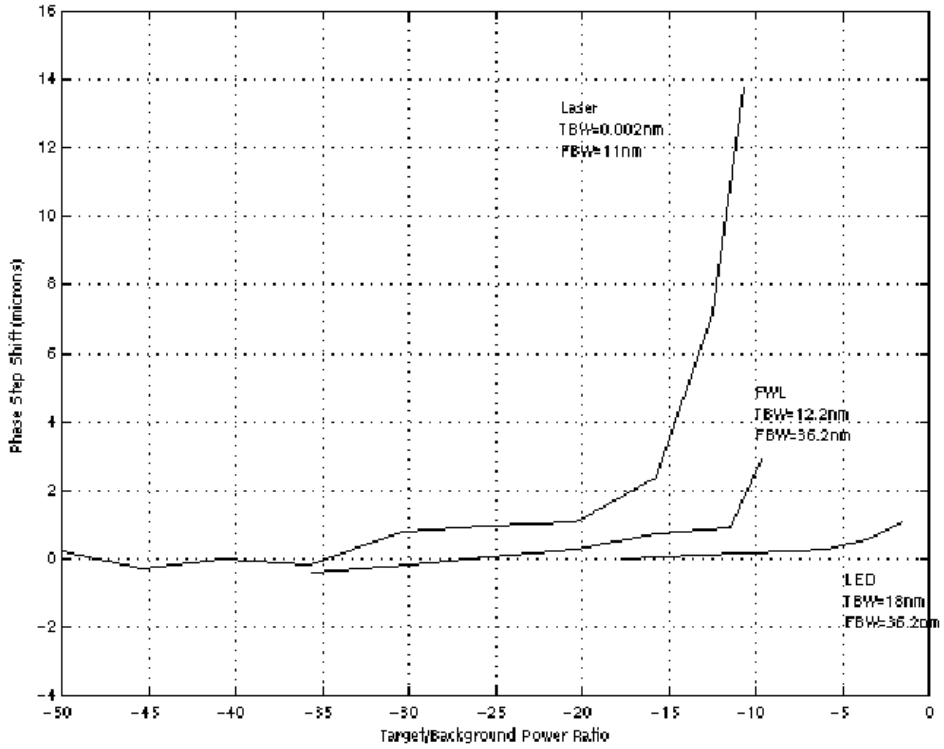

Figure 9 - Sensitivity of various emitters and filters

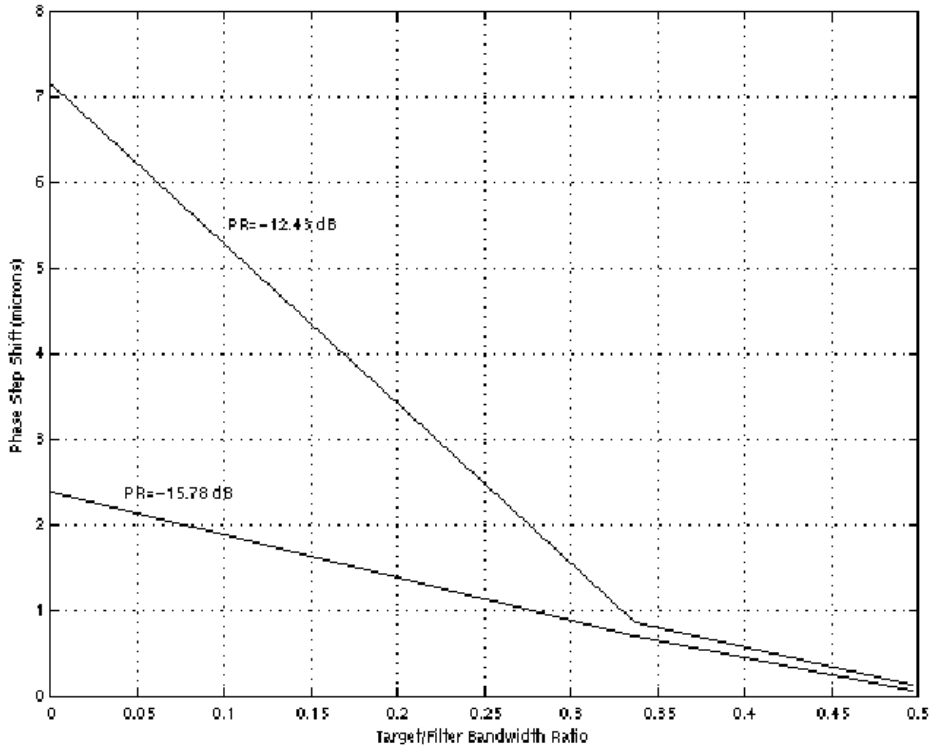

Figure 10- Sensitivity variation with Power and bandwidth ratios

6. CONCLUSION

This paper describes the performance of an interferometric system with different emission sources and filtering schemes. The results show that a very high sensitivity (-49 dB), relative to the background power before the filter, can be achieved when detecting coherent emission sources such as a laser with a coherence length of about 20 cm. High sensitivities (-32 dB and -24 dB) are also achievable when detecting partially coherent emission sources, such as the ones used in our experiments, with coherence lengths of 34 and 23 microns respectively. The sensitivity of our system increases with coherence length. This technique is expected to be useful in situations were narrow, but only partially coherent spectral lines need to be detected, not only in the emission case studied here, but also for absorption and reflection generated features, such as the ones generated by gases in the atmosphere or organic molecules in human tissue.

7. ACKNOWLEDGEMENTS

The authors thank Duleep Wickramasinghe from DERA Portsdown, UK for helpful discussions and for lending part of the optical equipment used in the experiments, Prof. Hugh Griffiths for providing this research direction and for arranging research funding, and the Brazilian Navy for sponsoring the first author.

8. REFERENCES

1. K. Chenosis and D. Harris, "Low Emissivity Camouflage Coatings", *Army Research Laboratory report* NR. ARL-TR-1095, 1996.
2. H. Schleijpen, "Evaluation of Infrared Signature Suppression of Ships", *Proc. Of the SPIE* vol. 2742, pp.245-254, 1996.
3. K. McCamey, R. Marko, L. Garvin and T. Peli, "Detection in Clutter Enhancement", *Proc. Of the SPIE 2742, pp. 225-235, 1996.*
4. H.A. French, "Apparatus and Method for Remote Sensing of Gases, Vapours or Aerosols", UK patent NR. 8406690.
5. R. Coutinho, H.A. French, D.R. Selviah, D. Wickramasinghe, H. Griffiths, "Detection of Coherent Light in an Incoherent Background", *Proc. of the IEEE Lasers and Electro-Optics Society 12th Annual Meeting*, pp. 247-248, 1999.
6. E. Hecht, Optics, 3rd edition, New York, 1998.
7. E. Kreyszig, Advanced Engineering Mathematics, 6th Edition, John Wiley & Sons, New York, 1988.